Available online at www.sciencedirect.com
SCIENCE DIRECT®
International Journal of Heat and Mass Transfer 47 (2004) 2817–2830
International Journal of HEAT and MASS TRANSFER
www.elsevier.com/locate/ijhmt

The experimental research on microtube heat transfer and fluid flow of distilled water

Dorin Lelea [a,*], Shigefumi Nishio [b], Kiyoshi Takano [b]

[a] Faculty of Mechanical Engineering, University "Politehnica" of Timisoara, B-dul Mihai Viteazu nr. 1, 300222 Timisoara, Romania
[b] Institute of Industrial Science, The University of Tokyo, 4-6-1 Komaba Meguro-ku, Tokyo 153 – 8505, Japan

Received 29 January 2003; received in revised form 28 September 2003

Abstract

The experimental and numerical research on microchannel heat transfer and fluid flow was presented in the paper. Diameters of the microtubes were 0.1, 0.3 and 0.5 mm and the flow regime was laminar with *Re*-number range up to 800. The working fluid was distilled water and the tube material was stainless steel. The experimental setup was designed in such a way that the investigation of the average friction factor and developing heat transfer was possible. Due to the large scattering in the reported experimental results, the scope of this research was to make the accurate measurements and to compare the experimental heat transfer and fluid flow characteristics with numerical and theoretical results for the conventional tubes.

Keywords: Microchannel heat transfer; Experimental research; Distilled water; Joule heating

1. Introduction

The term "micro-channel" comes to be used in some engineering fields but its definition is dependent on researchers. As is well known, the conventional heat transfer theory predicts that heat transfer coefficient of fully developed laminar flow in a channel increases if the cross-section of the channel decreases [1]. Tubes or channels of smaller size are therefore chosen to attain a high heat transfer coefficient. For example, such tubes or channels are used to manage the power dissipation in LSI chips. On the other hand, μ-TAS (Micro Total Chemical Analyzing System) [2], MEMS (Micro Electrical–Mechanical Systems) and bio-chips [3] consist of the network of channels of small cross-sectional size manufactured with microprocessing techniques. To develop such systems, we have to obtain a good understanding of flow and diffusion characteristics. In the present report, the tubes or channels utilized in such fields are called "microchannels". In the past decade, a large number of research reports considering microchannel heat transfer, have been presented. Since the topic of the present research was water flow and heat transfer, only reports on liquid as the working fluid will be reviewed.

Celata et al. [4], investigated experimentally single-phase heat transfer of R 114 in a stainless steel tube of the diameter $D = 0.130$ mm. They have found that friction factor is in good agreement with the Hagen–Poiseuille theory [5] as far as the *Re*-number is below 583. For heat transfer characteristics, they have found that *Nu* is not constant but depends on *Re*.

Mala et al. [6], experimentally investigated the flow characteristics of water through microtubes of $D_i =$ 50–254 μm. Two types of microtubes are used, and they are silica fused and stainless steel tubes. It is observed that for low values of *Re* the experimental data of *fRe* agree well with a theory. On the other hand with increasing *Re* significant deviation from the conventional theory comes to be observed. Also, this deviation increases as the tube diameter decreases. They reported also an early transition from the laminar to turbulent flow.

* Corresponding author. Tel.: +40-256-403670; fax: +40-256-403669.
E-mail address: ldorin@mec.utt.ro (D. Lelea).

0017-9310/$ - see front matter © 2004 Elsevier Ltd. All rights reserved.
doi:10.1016/j.ijheatmasstransfer.2003.11.034

Nomenclature

A_f	frontal cross-section, m^2
A_c	core cross-section, m^2
c_p	specific heat capacity, J/kg K
D_h	hydraulic diameter of a microtube, m
D_i	inner diameter of a microtube, m
D_o	outer diameter of a microtube, m
D_1	inner diameter of the tube before microtube, m
D_2	inner diameter of the tube after microtube, m
f	friction factor, –
fRe	friction constant, –
G	mass velocity inside the microtube, kg/m^2s
h	heat transfer coefficient, W/m^2 K
k_f	thermal conductivity of the water, W/m K
k_s	thermal conductivity of SUS 304, W/m K
K_c, K_e	contraction and expansion coefficients, respectively
L_{tot}	total length of the microtube, m
L_h	heating length of the microtube, m
L_n	distance between thermocouples, m
L_1	length of the inlet portion of the tube before microtube, m
L_2	length of the outlet portion of the tube after microtube, m
M	mass flow rate, kg/s
Nu	local Nusselt number, –
Pr	Prandtl number, –
Δp	total pressure drop, Pa
Δp_f	pressure drop due to the friction inside a tube, Pa
Δp_a	pressure drop due to the acceleration of the fluid, Pa
Δp_c	pressure drop due to the contraction of the cross-section area, Pa
Δp_e	pressure drop due to the expansion of the cross-section area, Pa
Δp_1	pressure drop due to the friction inside the tube before microtube, Pa
Δp_2	pressure drop due to the friction inside the tube after the microtube, Pa
Q, Q_{in}	heat transfer rate generated by the electrical power, W
Q_{out}	heat transfer rate removed by water, W
q	heat flux, W/m^2
r	radial coordinate, m
Re	Reynolds number, –
S_c	internal heat source, W/m^3
T_{wn}, T'_{wn}	wall temperature at different axial locations inside and outside the tube respectively, K
T_{bn}	water bulk temperature at the axial positions of the thermocouple measurements, K
T_{in}, T_{out}	inlet and outlet water temperature respectively, K
u, v	velocity components, m/s
u_m	water average velocity, m/s
z	axial coordinate, m

Greek symbols

δ	width of the microtube wall, m
ε	heat balance of the experimental setup, –
ρ	density, kg/m^3
σ	cross-section ratio, A_c/A_f, –
μ	viscosity, Pa s

Subscripts

f.d.	fully developed
in	inlet
i	inner
out	outlet
o	outer

Judy et al. [7], examined experimentally the flow characteristics of water, hexane and isopropanol, in fused silica microtubes with $D_i = 20$–150 μm for $Re = 20$–2000. Their results indicated that the values of fRe agree well with the conventional Stokes flow theory [5] for $D_i = 100$ and 150 μm. For $D \leqslant 75$ μm, the experimental results deviates from the conventional value of $fRe = 64$ towards lower values, although it preserved a constant value over the tested range of Re.

Li et al. [8], investigated experimentally the flow characteristics of deionized water in the glass ($D_h = 79.9$–166.3 μm), silicon ($D_h = 100.25$–205.3 μm) and stainless steel tubes ($D_h = 128.76$–179.8 μm). The length of the tubes was long enough to ensure that the flow is fully developed. They have found that there is no difference from the conventional and the value of fRe is almost 64 for the smooth tubes made of glass or silicon, and 15–37% higher than 64 for the stainless steel tubes. The transition from laminar to turbulent flow is observed in the range $Re = 1700$–2000.

Yang et al. [9], examined experimentally the flow characteristics of water, R-134a and air in small tubes of $D_h = 0.171$–4.01 mm for the laminar and turbulent flow regimes. The laminar-turbulent transition was observed in the range of $Re = 1200$–3800 and it is increasing with decreasing the tube diameter. The friction factor, in the case of liquids, agrees well with conventional Blausius and Poiseuille equations in the turbulent and laminar regime, respectively.

Peng and Peterson [10], investigated the heat transfer and flow characteristics of methanol and water. Microchannels of four different sizes are used, with a channel width ranging from 0.31 to 0.75 mm. The transition from the laminar flow occurs at $Re = 300$, and to the fully turbulent flow at $Re = 1000$.

Qu et al. [11], investigated the heat transfer of water flows through trapezoidal silicon microchannels. They have found that *Nu* number is much lower than conventional theoretical values.

Peng and Peterson [12], investigated experimentally heat transfer through rectangular microchannels with binary mixtures of water and methanol as a working fluid. They have analyzed both the influence of mixture concentration and channel geometry on heat transfer coefficient. They also found early transition from the laminar to turbulent regime, and the critical *Re*-number decreases as the hydraulic diameter of the channel decreases.

Peng and Peterson [13], investigated experimentally both the laminar and turbulent heat transfer and fluid flow characteristics of water through microchannels with $D_h = 0.133$–0.367. They have found a strong dependence of heat transfer and hydrodynamic characteristics on the channel size.

Gao et al. [14], investigated experimentally the heat transfer and flow characteristics of demineralized water flows through microchannels with $D_h = 0.1$–1 mm. The friction factor was in good agreement with conventional theoretical results for channels but the experimental data of *Nu* are much lower than the conventional theoretical results for smaller values of D_h.

Agostini et al. [15], investigated experimentally the heat transfer and flow characteristics of R134a through a multichannel configuration with $D_h = 0.77$ and 1.17 mm. In the case of the friction factor results there is a reasonable agreement with conventional theoretical results, both in the laminar and the turbulent regime. However, the experimental results of *Nu* are dependent on *Re* for both laminar and turbulent regimes.

Considering the available results about experimental research on microchannel heat transfer and fluid flow characteristics, one can conclude that there is a large scattering in the obtained results. This is especially serious in the case of the heat transfer results. For example, there is an optimum size of channels in the so-called microchannel heat sink and the result of optimization depends strongly on the heat transfer characteristics in microchannels. So, this was the reason for making the research on single-phase microtube heat transfer.

2. Description of the experimental setup

The experimental setup, used in the present study, was designed in the way that it allows the analysis of a developing heat transfer and fluid flow. The schematic view of the experimental apparatus is presented in Fig. 1.

Distilled water is the working fluid that is driven in a microtube with a micropump (NS type NP–KX–110) for volume flow rates 0.01–10 ml/min. A microchannel is placed inside a vacuum chamber to eliminate heat loss to ambient. The temperature of water, at the inlet of the microtube was kept at a prescribed value by using a counter-flow heat exchanger, placed before the microchannel. Water was circulated between the heat exchanger and a constant temperature bath to maintain the inlet temperature. Filters of 2 μm were set both before the microchannel and before the pump, for suppressing particles to enter inside the test tube.

The microtube was heated by Joule heating with an electrical power supply (Yokogawa 2558) and the input

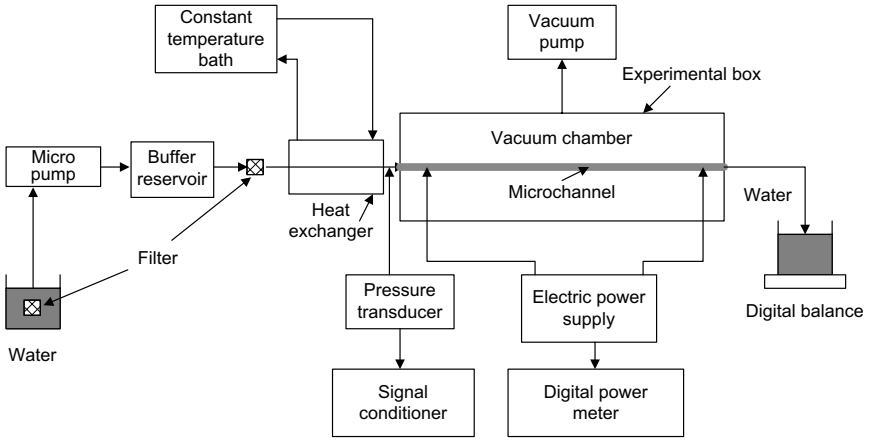

Fig. 1. Schematic representation of the experimental setup.

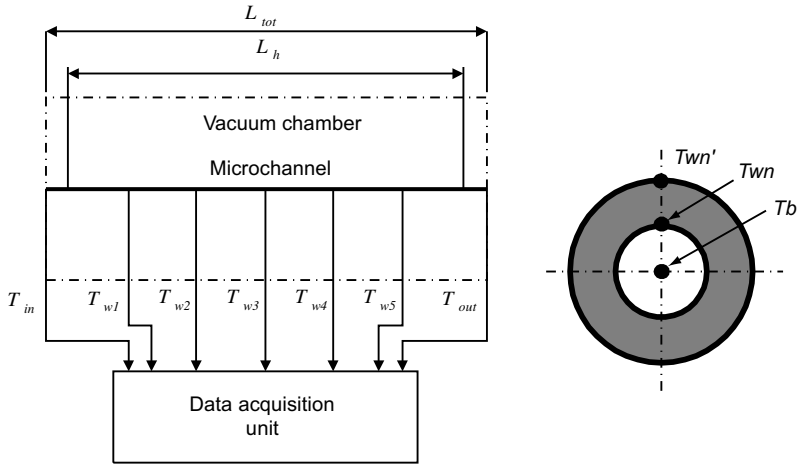

Fig. 2. The position of the thermocouples.

Table 1
Tube geometry description

Tube no.	D_i/D_o [μm]	Heating length L_h [mm]	Total length L_{tot} [mm]	Heat input Q [W]	Heat rate q_o [W/m^2]
1	500/700	250	600	0 and 2	3640
2	300/500	95	123	0, 1 and 2	6705 and 13 409
3	125.4/300	53	70	0, 0.5 and 0.75	10 015 and 15 022

heat was measured by a digital power meter (Yokogawa WT 200). The electrodes connected to the microtubes have a diameter of $d = 250$ μm. In the present experiments, the exit of the tube was kept at the atmospheric pressure. So, the pressure drop through the microtube was determined by measuring the pressure at the inlet of the test section with a pressure transducer (Kyowa PGM 2 KC and PGM 5 KC). The mass flow rate was determined by measuring the weight of water flowing out from the tube with a digital balance.

The mean temperature of water was measured at both the entrance and the exit cross-section of the experimental setup using K-type thermocouples. The same type thermocouples were used for measuring outer wall temperatures of the microtube. The diameter of all thermocouples was 50 μm and the thermocouple locations are presented in the Fig. 2.

The tubes were made of stainless steel SUS 304 and the experimental conditions are listed in Table 1. The tubes were heated electrically dissipating the heat in the range $Q = 0.5$–2 W.

3. Data reduction

The friction factor is calculated by Eq. (1) based on the experimental data of mass flow rate and the pressure drop due to the friction inside the microtube Δp_f,

$$f = \frac{L_{tot}}{D_i}\frac{\Delta p_f}{\frac{\rho \cdot u_m^2}{2}} \tag{1}$$

On the other hand, in the present experiment the total pressure drop along the test section is measured. The total pressure drop includes the pressure drop at the inlet and outlet portion of the experimental setup, pressure drop due to the contraction and expansion of the cross-sectional area, pressure drop required for acceleration of the fluid and frictional pressure drop. So, the total pressure drop Δp, can be expressed with the following equation:

$$\Delta p = \Delta p_c + \Delta p_1 + \Delta p_{core} - \Delta p_e + \Delta p_2 \tag{2}$$

The pressure drop through the tube, Δp_{core} is expressed by the following equation:

$$\Delta p_{core} = \Delta p_f + \Delta p_a \tag{3}$$

Here, Δp_a, is the pressure drop due to acceleration of the fluid and given by,

$$\Delta p_a = \frac{G^2}{\rho_{in}}\left(\frac{\rho_{in}}{\rho_{out}} - 1\right) \tag{4}$$

Pressure drop due to the contraction is calculated by

$$\Delta p_c = \frac{G^2}{2 \cdot \rho_{in}}\left(1 - \sigma^2 + K_c\right) \tag{5}$$

Pressure drop due to the expansion is calculated by the following equation

$$\Delta p_e = \frac{G^2}{2 \cdot \rho_{out}}\left(1 - \sigma^2 - K_e\right) \tag{6}$$

The coefficients K_c and K_e respectively, depends on σ and Re and can be obtained from [5].

Pressure drop at the inlet portion of the experimental setup is defined as

$$\Delta p_1 = \frac{128 \cdot M \cdot L_1 \cdot v_{in}}{\rho_{in} \cdot \pi \cdot D_1^4} \tag{7}$$

Pressure drop at the outlet portion of the experimental setup is defined as

$$\Delta p_2 = \frac{128 \cdot M \cdot L_2 \cdot v_{out}}{\rho_{out} \cdot \pi \cdot D_2^4} \tag{8}$$

The local value of Nu is calculated by the following equation:

$$Nu = \frac{h \cdot D_i}{k_f} \tag{9}$$

where h is the local heat transfer coefficient defined by the following equation:

$$h = \frac{q}{T_{wn} - T_{bn}} \tag{10}$$

where T_{bn} is the local bulk temperature of water at each point of the wall temperature measurement and it is calculated from the heat balance equation:

$$T_{bn} = T_{in} + \frac{\pi \cdot D_i \cdot L_n \cdot q}{M \cdot c_p} \tag{11}$$

T_{wn} is the local wall temperature at the inside of the tube and it is obtained from the one-dimensional heat conduction equation using the measured wall temperature at the outside of the microtube:

$$\frac{d^2T}{dr^2} + \frac{1}{r}\frac{dT}{dr} + \frac{S_c}{k_s} = \frac{1}{r}\frac{d}{dr}\left(r\frac{dT}{dr}\right) + \frac{S_c}{k_s} = 0 \tag{12}$$

where S_c is the internal heat source generated inside the microtube wall by the electric power defined as:

$$S_c = \frac{Q}{L_h \cdot \pi \cdot (R_o^2 - R_i^2)} \tag{13}$$

After integration the general solution of the Eq. (12) is obtained:

$$T = -\frac{r^2}{4}\frac{S_c}{k_s} + C_1 \ln r + C_2 \tag{14}$$

Constants C_1 and C_2 can be obtained by the following boundary conditions:

$$r = R_o \quad T = T'_{wn}$$

$$r = R_i \quad k_s \frac{dT}{dr} = q_i = \frac{Q}{2R_i \pi L_h} = \frac{S_c}{2}\frac{R_o^2 - R_i^2}{R_i}$$

Finally, the local temperature at the inside portion of the microtube wall is obtained by the following equation:

$$T_{wn} = T'_{wn} - \frac{S_c}{4k_s}\left[R_o^2 \ln\left(\frac{R_o}{R_i}\right)^2 - (R_o^2 - R_i^2)\right] \tag{15}$$

It should be noted that the fluid properties were estimated at the average temperature of water and they were obtained from Computer package PROPATH v. 10.2.

Finally, Re is calculated by the following equation:

$$Re = \frac{\rho \cdot u_m \cdot D_i}{\mu} \tag{16}$$

4. Experimental uncertainties

The uncertainty of experimental results have been estimated following the recommendations and method described by Moffat [16,17]. Analyzing the particular uncertainty results that the main problem is the accuracy of the friction constant results as the outcome of difficulties on determining the inner diameter of the microtube. We can measure the inner diameter of the tubes tested, using the following two methods. One of them was to measure the inner diameter at both ends of microtubes by a high-precision microscope. A disadvantage of this method is the lack of the information on diameter distribution along the tube axes. The other

Table 2
The experimental uncertainties

Parameter	Uncertainty [%]		
	$D_i = 125.4$ μm	$D_i = 300$ μm	$D_i = 500$ μm
Inner diameter, D_i	5.6	0.98	0.4
Mass flow rate, M	0.04	0.04	0.04
Re-number	5.3	0.98	0.4
Friction factor f	18.7	3.9	1.5
Local temperature difference, ΔT_{loc}	5.9	2.8	7.9
Local heat transfer coefficient, h	8.9	3.6	8.9

method was to obtain the average inner diameter of the microtube by measuring the mean outer diameter, length and weight of the tube, and the mean inner diameter was determined by using the density of tube material. In this case the accuracy is affected by the accuracy of the three additional parameters stated above. In the present research the later method was used and the uncertainties of some particular parameters, affected by the uncertainty of the inner diameter, are presented in Table 2.

5. Numerical details

In order to discuss experimental results obtained in the present experiments, the velocity and temperature distributions were numerically solved taking account of the temperature variation of fluid properties.

As mentioned already, in the experimental setup, there were two electrodes at both ends of the test tube. So, as shown in Fig. 3, the respective insulated parts were included in the numerical domain. The following set of partial differential equations is used to describe the phenomena:

Continuity equation:

$$\frac{\partial u}{\partial z}+\frac{1}{r}\frac{\partial(r\cdot v)}{\partial r}=0 \tag{17}$$

Momentum equation:

$$\rho\cdot\left(v\frac{\partial u}{\partial r}+u\frac{\partial u}{\partial z}\right)=-\frac{\mathrm{d}p}{\mathrm{d}z}+\frac{1}{r}\frac{\partial}{\partial r}\left(\mu(T)r\frac{\partial u}{\partial r}\right) \tag{18}$$

Energy equation:

$$\rho\cdot c_p\cdot\left(v\frac{\partial T}{\partial r}+u\frac{\partial T}{\partial z}\right)=k\cdot\left[\frac{1}{r}\frac{\partial}{\partial r}\left(r\frac{\partial T}{\partial r}\right)+\frac{\partial^2 T}{\partial z^2}\right] \tag{19}$$

At the inlet of the tube, the uniform velocity and temperature field is considered, while at the exit the temperature gradient is equal to zero.

The boundary conditions are:

$$z=0,\quad 0<r<R_{\mathrm{o}}:\quad u=u_0,\ T=T_w=T_0$$

$$0<z<L_{\mathrm{tot}}:\quad r=0,\ \frac{\partial u}{\partial r}=0,\ \frac{\partial T}{\partial r}=0,\ v=0$$

$$r=R_{\mathrm{i}},\quad u=v=0$$

The Joule heating of the tube wall can be expressed either by the uniform heat generation through the tube wall or by the uniform heat flux imposed on the outer surface of the wall. For the latter case, the boundary condition is defined as,

$$r=R_{\mathrm{o}}:\quad q_{\mathrm{o}}=k_{\mathrm{s}}\frac{\partial T}{\partial r}\quad\text{(for the heated portion of the tube)}$$

$$k_{\mathrm{s}}\frac{\partial T}{\partial r}=0\quad\text{(for the insulated portion of the tube)}$$

where q_{o} is the heat flux based on the outer heat transfer area of the tube wall (Table 1).

$$z=L_{\mathrm{tot}},\quad 0<r<R_{\mathrm{o}}:\quad \frac{\partial T}{\partial z}=0$$

The partial differential equations (17)–(19) together with boundary conditions, are solved using the finite volume method described in [18].

First, the parabolic flow field condition is considered and the velocity field is solved. The temperature field, as a conjugate heat transfer problem, was then solved using the obtained velocity field. The fluid flow regime is considered to be a steady-state laminar flow with constant fluid properties except for the fluid viscosity that is calculated with following equation:

$$\mu=\mu_0\cdot\mathrm{e}^{\beta(T-T_0)} \tag{20}$$

In order to test the grid sensitivity, two grids have been used. The coarser one with 250 cells in radial direction and 400 cells in axial direction and finer grid with 500 and 800 cells in z- and r-direction respectively. Differences in the results of fRe or Nu were smaller than

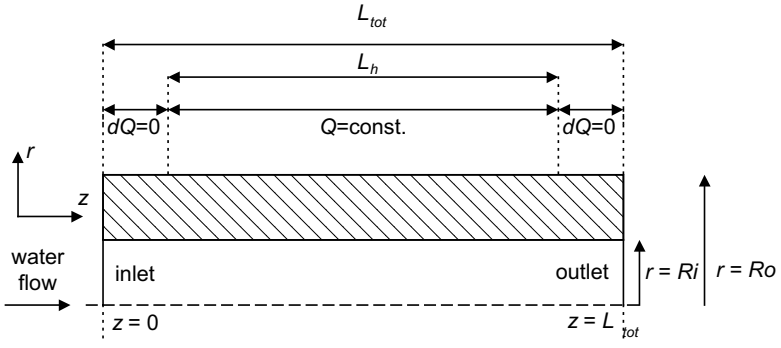

Fig. 3. Schematic presentation of the test tube.

0.1%, so the coarser grid has been used for further calculations.

6. Results and discussion

6.1. Hydrodynamic results

6.1.1. Hydrodynamic results for no-heating fluid flow

The pressure drop from the inlet of the tube up to some axial location can be expressed with the following equation:

$$\frac{\Delta p(z)}{(\rho \cdot u_m^2)/2} = \frac{\Delta p(z)_{f.d.}}{(\rho \cdot u_m^2)/2} + K(z) \tag{21}$$

where $\Delta pz_{f.d.}$ is the pressure drop in the case of the fully developed flow and $K(z)$ is the incremental pressure drop due to the entrance region effects. Eq. (21) can also be written in the following form:

$$\frac{\Delta p(z)}{(\rho \cdot u_m^2)/2} = fRe_{f.d.}\left(\frac{z}{D_i \cdot Re}\right) + K(z) \tag{22}$$

For a very long tubes (as in the present experiments), the incremental pressured drop for a laminar flow inside the tubes has the following value [19]:

$$K(\infty) = 1.25$$

Finally the fully developed value of the $fRe_{f.d.}$ can be obtained from the Eq. (22).

The numerical and experimental results of $fRe_{f.d.}$ for $D_i = 300$ and 125.4 μm are plotted to Re in Figs. 4 and 5 respectively. In these figures, the no-heating fluid flows are considered.

As seen from Figs. 4 and 5, the obtained results for $fRe_{f.d.}$ are in good agreement with the conventional theoretical value of $fRe = 64$. There is a difference between the experimental and numerical results but this difference is much lower than the experimental uncertainty of the measurements.

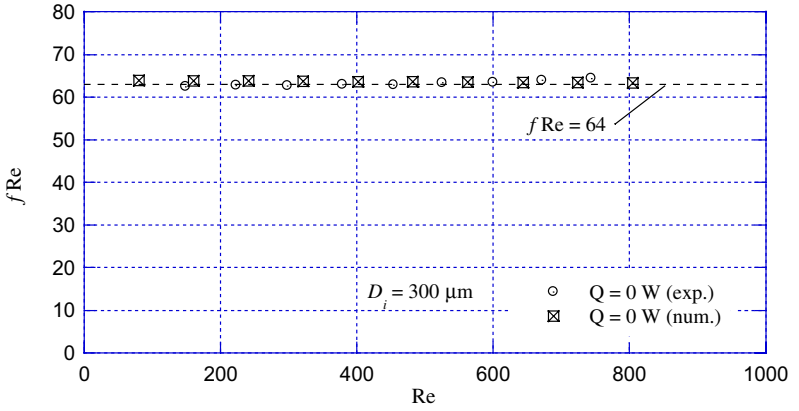

Fig. 4. Experimental and numerical results of fRe for no-heating fluid flow in tube of $D_i = 300$ μm.

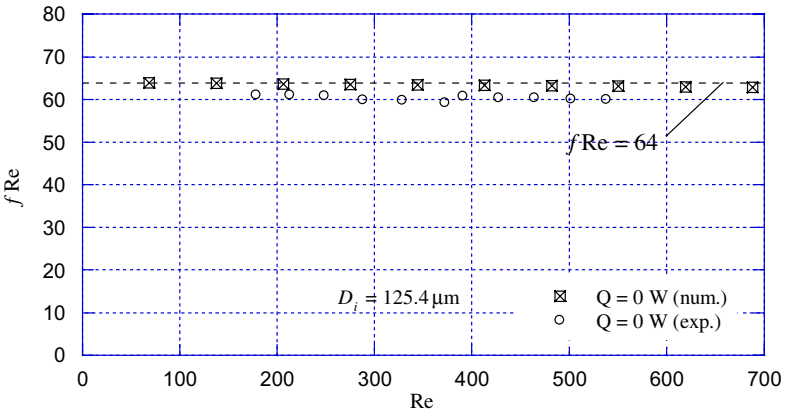

Fig. 5. Experimental and numerical results of fRe for no-heating fluid flow in tube of $D_i = 125.4$ μm.

In short, the present results indicate that the conventional relation of $fRe = 64$ is valid and there is also no evidence on an early transition from laminar to turbulent regime, at least for $D_i > 100$ μm and the Re range covered in the experiment.

6.1.2. Hydrodynamic results for different input power levels

The numerical and experimental results of fRe under heated conditions for $D_i = 300$ and 500 μm are presented in Figs. 6 and 7 respectively. In the case of the tube with $D_i = 300$ μm, regardless of the input power level, the value of fRe is almost constant both for the numerical and experimental results. It should be noted here that, as shown in Table 1, the heated portion of this tube was almost the same as the total length of the tube.

Contrary, in the case of the tube with $D_i = 500$ μm, the experimental value of fRe is decreasing with decreasing Re especially in the case of the lower Re where a larger temperature differences between the inlet and outlet of the tube are expected. This behavior of fRe is also confirmed by the present numerical results plotted in the figures. It should be noted here that, as shown in Table 1, the heated portion of this tube is significantly shorter than the total length and the fluid viscosity is evaluated at the arithmetic mean temperature between the inlet and outlet.

From Eqs. (1) and (15), the fRe can be defined as follows:

$$fRe = \frac{2 \cdot \Delta p \cdot D_i^2}{L_{tot} \cdot u_m \cdot \mu} \tag{23}$$

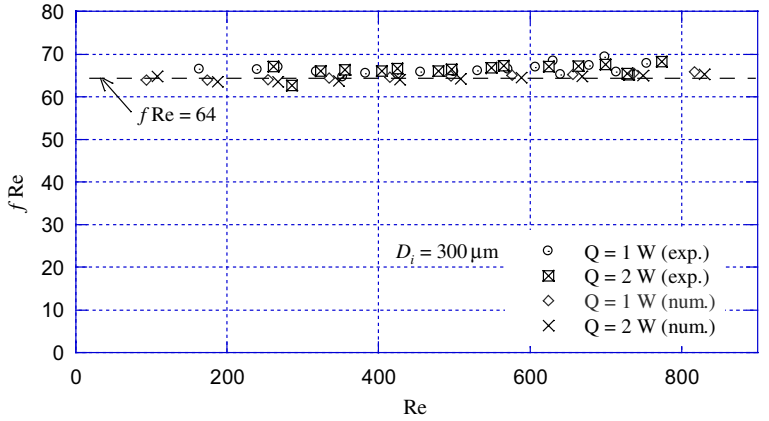

Fig. 6. Experimental and numerical results of fRe for different input powers in tube of $D_i = 300$ μm.

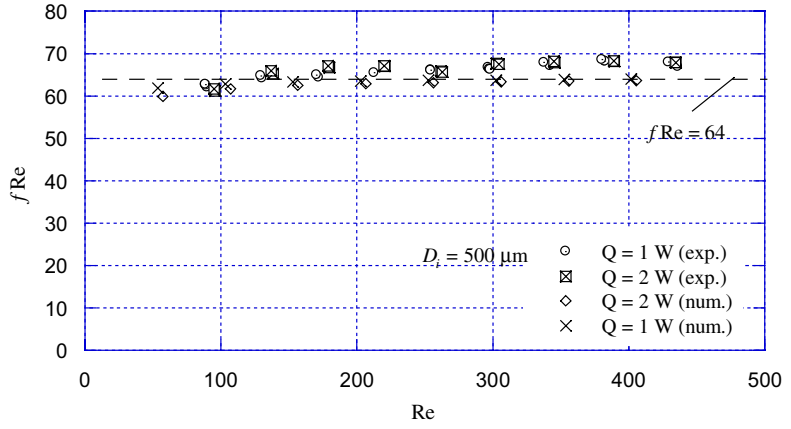

Fig. 7. Experimental and numerical results of fRe for different input powers in tube of $D_i = 500$ μm.

In the case of the no-heating fluid flow, the relationship between the pressure drop and the mean fluid velocity is linear, so the ratio $\Delta p/u_m$ has a constant value. In the case of the fluid flow under heated conditions, due to the lower wall shear stress, the pressure drop and the ratio $\Delta p/u_m$ is not constant but decreases exponentially. When the heated portion of the tube is almost the same as the total length of the tube, the ratio $\Delta p/u_m$ decreases almost at the same rate as the fluid viscosity, with decreasing the mean fluid velocity. Contrary, if the heated portion of the tube is significantly shorter than the total length of the tube, the ratio $\Delta p/u_m$ decreases faster with decreasing the mean fluid velocity, than a fluid viscosity. For the present experimental conditions, the changes in fluid density are negligible.

Taking this into account, the value of *fRe* will be constant only for the case when the total length of the tube is heated. In the case of the partial heating, the value of the *fRe* will be lower than the conventional relation $fRe = 64$.

6.2. Thermal results

To keep the experimental uncertainty within an allowable level for thermal results in a microtube, special care should be taken of the reduction of heat loss. In the present experiment, the followings were carried out to reduce the heat loss from the microtube. The room temperature was kept at the inlet temperature of water (about 20 °C) with an air-conditioning unit. As shown in Fig. 1, the microtube was placed in the vacuum chamber. The remaining way of heat transfer to the ambient was heat conduction through the electrodes connected to the tube wall as well as through the power wires connected to the digital power meter. This problem was especially serious in the case of the microtubes, and K-type thermocouples of 50 μm in diameter were chosen to minimize the amount of heat loss through five thermocouples placed on the tube wall.

The following value of ε was used as a measure of thermal uncertainty in the present experiment:

$$\varepsilon = \frac{Q_{out} - Q_{in}}{Q_{in}} \cdot 100 \tag{24}$$

where Q_{in} is the electrical input power, Q_{out} is the amount of heat transferred to water and this is given by,

$$Q_{out} = M \cdot c_p \cdot (T_{out} - T_{in}) \tag{25}$$

In Figs. 8 and 9, experimental results of ε were presented for microtubes $D_i = 125.4$ and 300 μm. From both figures it is clear that, as *Re* decreases, the absolute value of ε increases. The reason may be explained as follows: the outlet temperature of water increases for smaller *Re*. This results in an increase of the temperature of the electrode placed at the outlet and also results in an increase of heat conduction through it to the ambient.

If the heat input is very large, the heat losses are larger than an acceptable value. Contrary if the heat input is very low, the temperature difference between the tube wall and water is much lower than an acceptable level. Anyway, the results shown in Figs. 8 and 9, the value of ε is of ±5% and about ±10% for $D_i = 300$ and 125.4 μm respectively.

In Figs. 10–14, the experimental results of the local value of *Nu* are plotted to the axial location for the respective experimental conditions. The experimental data in Figs. 10–14 indicate that, as predicted by conventional heat transfer theories, the local *Nu* number defined by Eq. (9) decreases and approaches to the constant value of 4.36 with increasing *z*. In Figs. 15–20, they are plotted to the non-dimensional axial distance together with the present numerical result and the theoretical values of Shah and London [19]. As seen from Figs. 15–20, the present experimental data are in reasonable

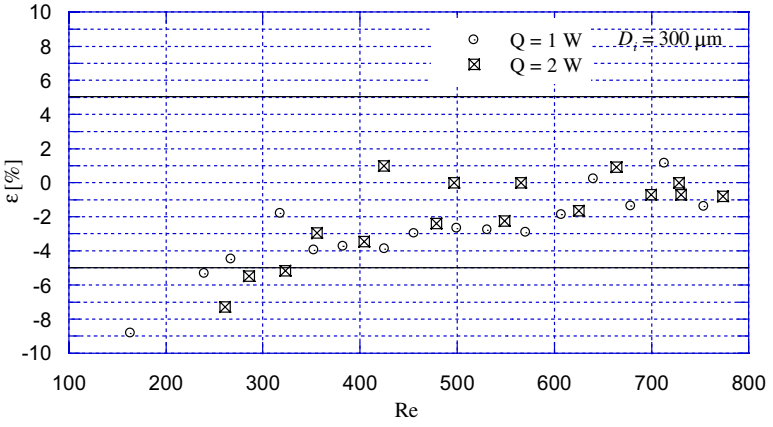

Fig. 8. Heat balance for tube of $D_i = 300$ μm.

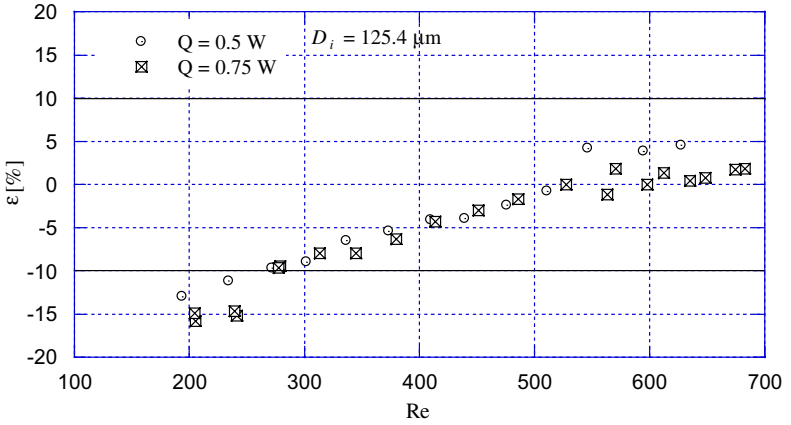

Fig. 9. Heat balance for tube of $D_i = 125.4$ μm.

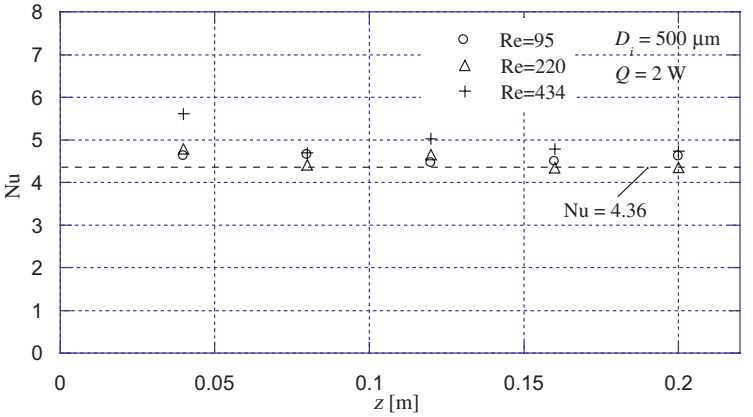

Fig. 10. Experimental results of local value of *Nu* for microtube of $D_i = 500$ μm and input power of $Q = 2$ W.

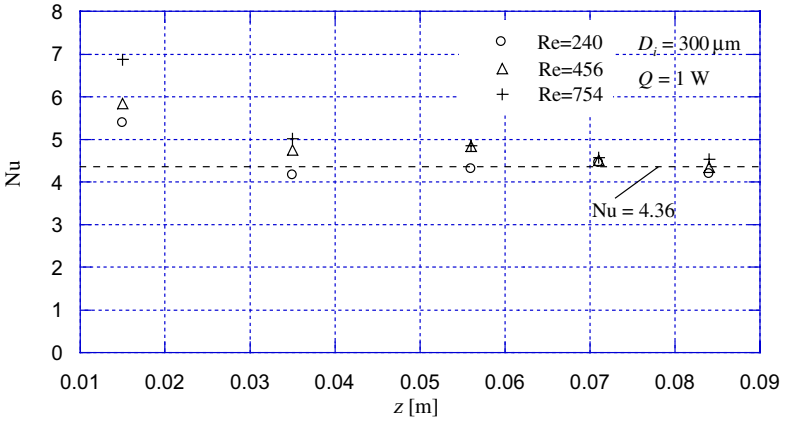

Fig. 11. Experimental results of local value of *Nu* for microtube of $D_i = 300$ μm and input power of $Q = 1$ W.

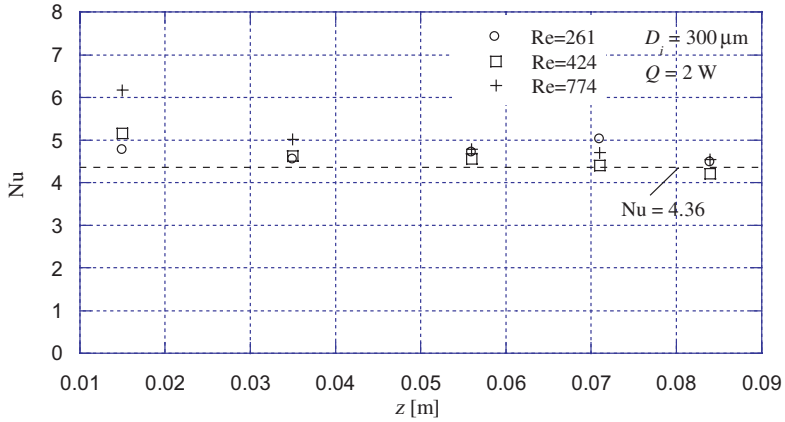

Fig. 12. Experimental results of local value of *Nu* for microtube of $D_i = 300$ μm and input power of $Q = 2$ W.

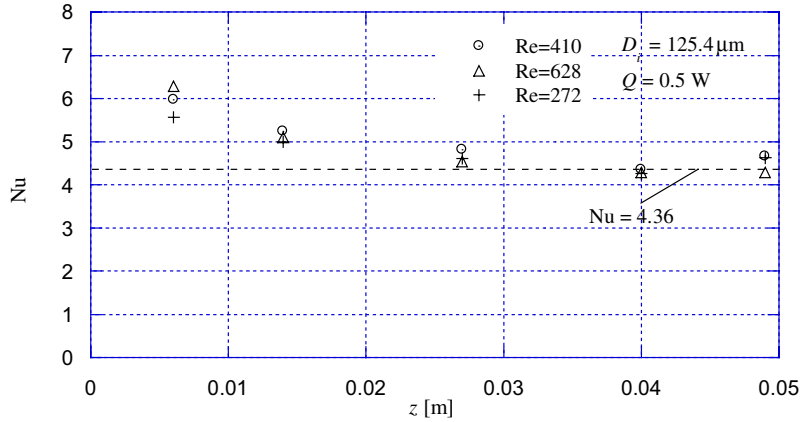

Fig. 13. Experimental results of local value of *Nu* for microtube of $D_i = 125.4$ μm and input power of $Q = 0.5$ W.

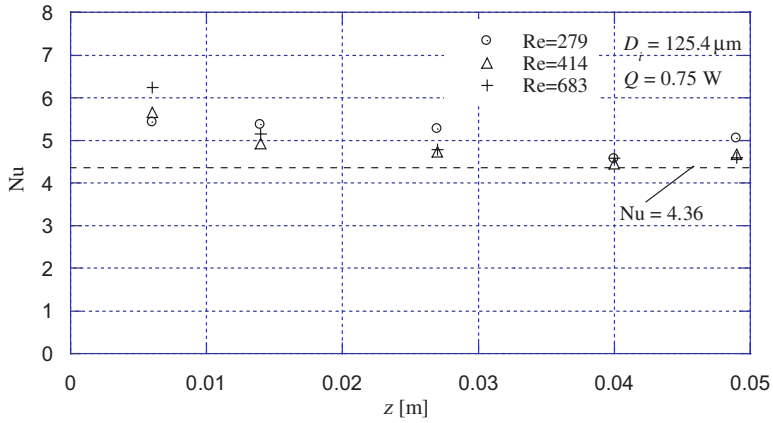

Fig. 14. Experimental results of local value of *Nu* for microtube of $D_i = 125.4$ μm and input power of $Q = 0.75$ W.

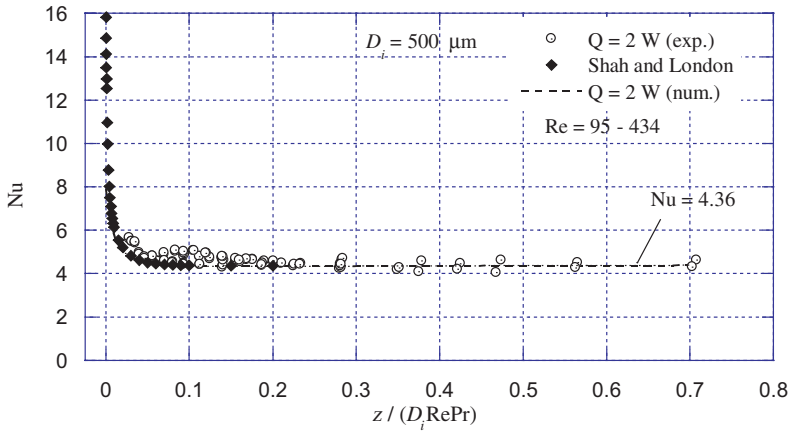

Fig. 15. Relation of local value of *Nu* to non-dimensional axial distance for microtube of $D_i = 500$ μm and input power of $Q = 2$ W.

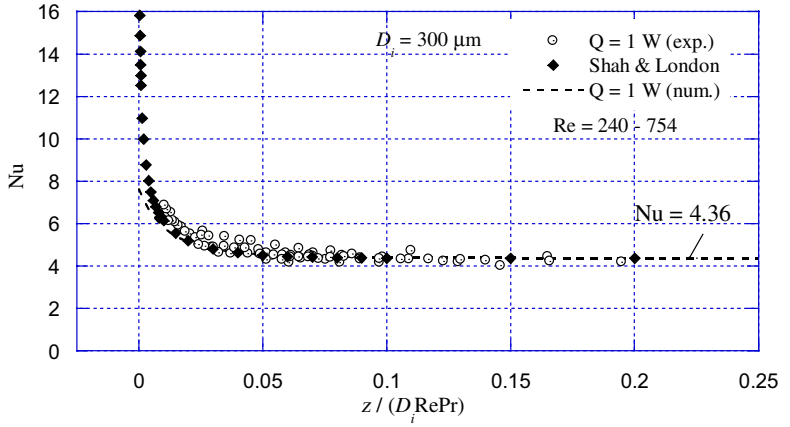

Fig. 16. Relation of local value of *Nu* to non-dimensional axial distance for microtube of $D_i = 300$ μm and input power of $Q = 1$ W.

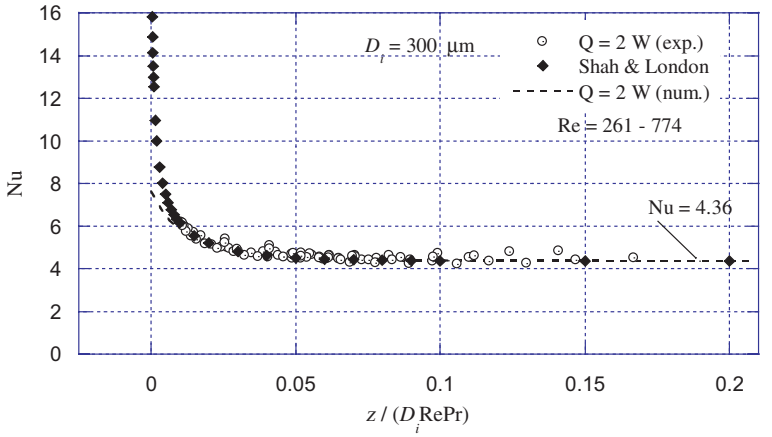

Fig. 17. Relation of local value of *Nu* to non-dimensional axial distance for microtube of $D_i = 300$ μm and input power of $Q = 2$ W.

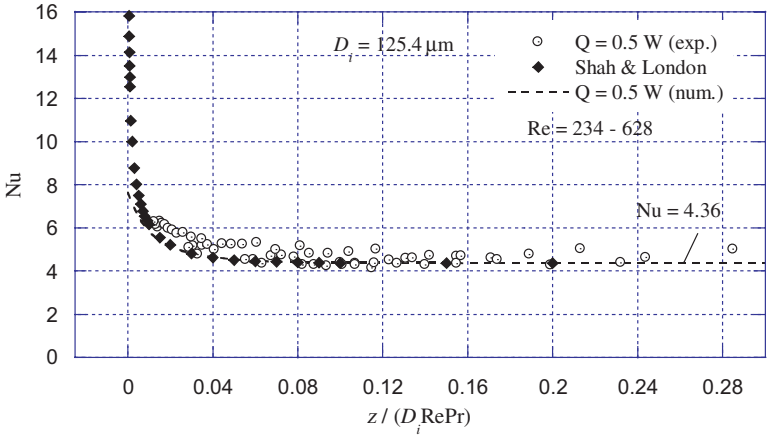

Fig. 18. Relation of local value of *Nu* to non-dimensional axial distance for microtube of $D_i = 125.4$ μm and input power of $Q = 0.5$ W.

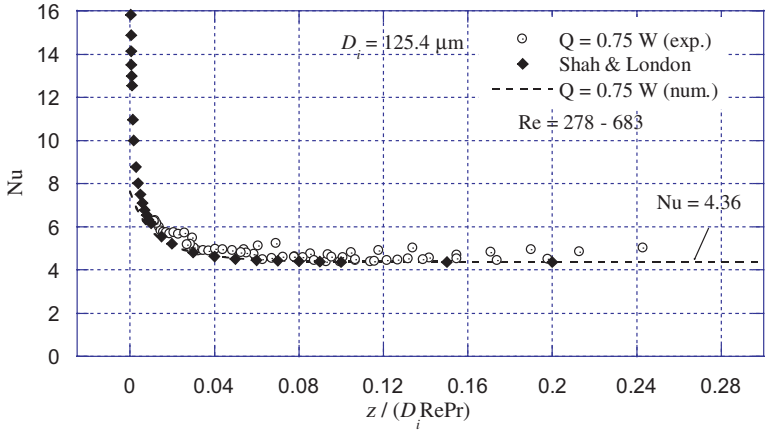

Fig. 19. Relation of local value of *Nu* to non-dimensional axial distance for microtube of $D_i = 125.4$ μm and input power of $Q = 0.75$ W.

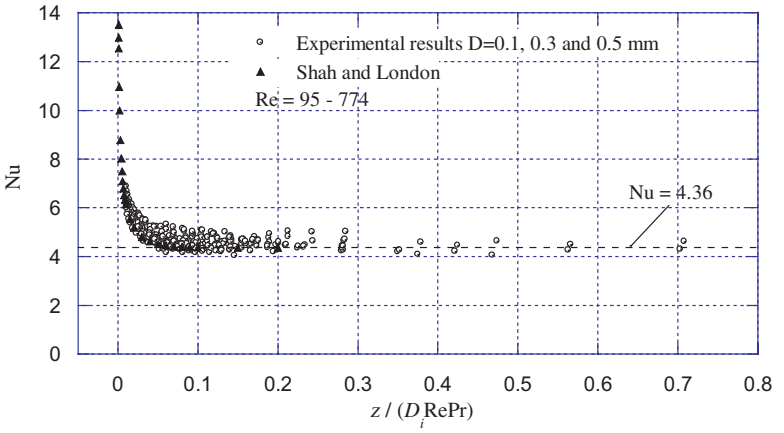

Fig. 20. Relation of local value of *Nu* to non-dimensional axial distance for microtubes of $D_i = 125.4$, 300 and 500 μm.

agreement with both the numerical and the theoretical results. In short, it can be concluded that, at least for the present experimental conditions, the local value of Nu is in good agreement with conventional theories including the entrance region.

7. Concluding remarks

A developing microchannel heat transfer and fluid flow has been analyzed experimentally on tubes of $D_i = 0.1$, 0.3 and 0.5 mm, having water as a working fluid. The experimental results have been compared both with theoretical predictions from literature and results obtained by numerical modeling of the present experiment. The experimental results of microchannel flow and heat transfer characteristics obtained in the present experiments confirms that, including the entrance effects, the conventional or classical theories are applicable for water flow through microchannel of above sizes.

This conclusion does not provide any new aspect, but this is meaningful considering the large scattering in the existing results.

References

[1] S. Nishio, Attempts to apply micro heat transfer to thermal management-invited lecture, in: International Conference on Heat Transfer and Transport Phenomena in Microscale, Banff, Canada, 2000, pp. 32–40.
[2] D.R. Reyes, D. Iossifidis, P.A. Auroux, A. Manz, Micro total analysis systems, introduction, theory and technology, Anal. Chem. 74 (12) (2002) 2623–2636.
[3] J. Lee, H. Moon, J. Fowler, C.J. Kim, T. Schoellhammer, Addressable micro liquid handling by electric control of surface tension, in: The 14th IEEE International Conference on Micro Electro Mechanical Systems 2001, MEMS 2001, 2001, pp. 499–502.
[4] G.P. Celata, M. Cumo, M. Guglielmi, G. Zummo, Experimental investigation of hydraulic and single phase heat transfer in 0.130 mm capillary tube, in: International Conference on Heat Transfer and Transport Phenomena in Microscale, Banff, Canada, 2000, pp. 108–113.
[5] A.F. Mills, Heat Transfer, Irwin Inc., 1992.
[6] G.M. Mala, D. Li, C. Werner, H.J. Jacobasch, Y.B. Ning, Flow characteristics of water through a microchannel between two parallel plates with electrokinetic effects, Int. J. Heat Fluid Flow 18 (5) (1997) 489–496.
[7] J. Judy, D. Maynes, W.B. Web, Liquid flow pressure drop in microtubes, in: International Conference on Heat Transfer and Transport Phenomena in Microscale, Banff, Canada, 2000, pp. 149–154.
[8] Z.X. Li, D.X. Du, Z.Y. Guo, Experimental study on flow characteristics of liquid in circular micortubes, in: International Conference on Heat Transfer and Transport Phenomena in Microscale, Banff, Canada, 2000, pp. 162–167.
[9] C.Y. Yang, H.T. Chien, S.R. Lu, R.J. Shyu, Friction characteristics of water, R-134a and air in small tubes, in: International Conference on Heat Transfer and Transport Phenomena in Microscale, Banff, Canada, 2000, pp. 168–174.
[10] X.F. Peng, G.P. Peterson, Convective heat transfer and flow friction for water flow in microchannel structures, Int. J. Heat Mass Transfer 39 (12) (1996) 2599–2608.
[11] W. Qu, G.M. Mala, D. Li, Heat transfer for water flow in trapezoidal silicon microchannels, Int. J. Heat Mass Transfer 43 (21) (2000) 3925–3936.
[12] X.F. Peng, G.P. Peterson, Forced convection heat transfer of single-phase binary mixtures through microchannels, Exp. Thermal Fluid Sci. 12 (1) (1996) 98–104.
[13] X.F. Peng, G.P. Peterson, The effect of thermofluid and geometrical parameters on convection of liquid through conventional microchannel, Int. J. Heat Mass Transfer 38 (1) (1995) 127–137.
[14] P. Gao, S. Person, M. Marinet, Hydrodynamics and heat transfer in a two-dimensional microchannel, in: Twelfth International Heat Transfer Conference, Grenoble France, 18–23 August, vol. 2, 2002, pp. 183–188.
[15] B. Agostini, B. Watel, A. Bontemps, B. Thonon, Experimental study of single-phase friction factor and heat transfer coefficient in mini-channels, in: International Symposium on Compact Heat Exchangers, Grenoble France, 24 August 2002, pp. 110–115.
[16] R.J. Moffat, Using uncertainty analysis in the planning of an experiment, J. Fluids Eng. 107 (1985) 173–179.
[17] R.J. Moffat, Contributions to the theory of single-sample uncertainty analysis, J. Fluids Eng. 104 (1982) 173–179.
[18] S.V. Patankar, Numerical Heat Transfer and Fluid Flow, McGraw Hill, 1980.
[19] R.K. Shah, A.L. London, Laminar Flow Forced Convection in Ducts, Advances in Heat Transfer—Supplement 1, Academic Press, New York, 1978.